

A new concept regarding the cause of ionosphere semiannual and annual anomalies

Francisco Azpilicueta¹ and Claudio Brunini¹

Received 28 July 2010; revised 25 September 2010; accepted 21 October 2010; published 20 January 2011.

[1] Since the beginning of the pioneering scientific work on the ionosphere, unusual responses have been reported and have been named semiannual and annual anomalies owing to their unexplained and periodic nature. Despite more than 60 years of scientific and technological achievements, a definitive explanation for these intriguing phenomena has not been found, and, on the contrary, similar anomalies have been found in other geophysical phenomena. The best candidate for the driving force behind the anomalies is the solar wind, but contemporary theories of the behavior of Earth's magnetosphere preclude the description of a causal mechanism. Here we present a mechanism of energy transfer from the magnetosphere to the ionosphere that can explain both anomalies. The importance of this theory is that it makes available a secondary source of energy to Earth's upper atmosphere and ionosphere; that energy could constitute as much as 40% of the energy budget in the ultraviolet and extreme ultraviolet regions of the solar electromagnetic spectrum. This will be of importance to thermospheric, ionospheric, magnetospheric, and space physics research.

Citation: Azpilicueta, F., and C. Brunini (2011), A new concept regarding the cause of ionosphere semiannual and annual anomalies, *J. Geophys. Res.*, 116, A01307, doi:10.1029/2010JA015977.

1. Introduction

[2] The purpose of this paper is to introduce a new theoretical physical framework with which to study and possibly explain two of the most widely studied phenomena that occur in the ionosphere: the semiannual and annual anomalies. The first reports concerning these so-called anomalies of the electron concentration in the upper atmosphere date back to the 1930s, to the pioneering works by Berkner *et al.* [1936] and Appleton [1938]. Since then several authors have proposed different approaches to understanding, modeling, and predicting these anomalies [Fuller-Rowell, 1998; Rishbeth, 1998, 2000; Li and Yu, 2003; Mendillo *et al.*, 2005]. However, the processes seemed to be so complex that no unique theory was able to model both effects, and many early theories could only partially explain one or the other.

[3] The physical framework discussed in this paper is as interesting as the anomalies themselves. The usual approximation of a stationary Earth magnetic field [Rossi and Olbert, 1970] (see also R. Fitzpatrick *et al.*, The Physics of Plasma, lecture notes for a graduate course, 2008, available at <http://farside.ph.utexas.edu/teaching/plasma/plasma.html>) for describing the movement of charged particles within the magnetosphere imposes a limiting factor for

explaining the anomalies. According to the results presented here, the $\sim 11^\circ$ tilt angle between Earth's magnetic and Earth's rotation axes produces, for a point not rotating with Earth, a time-varying magnetic vector that results in a dynamo force (that is called the Earth rotation dynamo force; ERDF). The effect of this force acting on the charged particles that compose the ring current surrounding Earth results in a mechanism by which ions (mainly) can penetrate Earth's magnetic field and spiral down to Earth's upper atmosphere. During their spiral descent the ions can interact with the neutral species, ions, and electrons present in upper atmospheric regions and produce the electron density enhancement associated with the anomalies. In other words, the ERDF provides a mechanism by which portions of the solar wind energy stored in the ring current can be transferred to the upper atmosphere and ionosphere.

[4] Finally, the ERDF theory can also be applied to other regions of the magnetosphere since it should be valid within the whole magnetosphere and can lead to a new way of interpreting space weather phenomena.

2. The Semiannual and Annual Anomalies

[5] During the first decades of ionospheric research in the twentieth century, the description of the ionospheric free electron vertical density, as well as its associated parameters such as the critical frequency of the F_2 ionospheric layer (f_oF_2), was mainly dominated by Chapman's theory [Chapman, 1931] of atmospheric ionization, in which the main driving variables were the solar irradiance level and the solar zenith angle from the observation point. Chapman's theory was successful in explaining several major char-

¹Facultad de Ciencias Astronómicas y Geofísicas, Universidad Nacional de La Plata, Consejo Nacional de Investigaciones Científicas y Técnicas (CONICET), La Plata, Argentina.

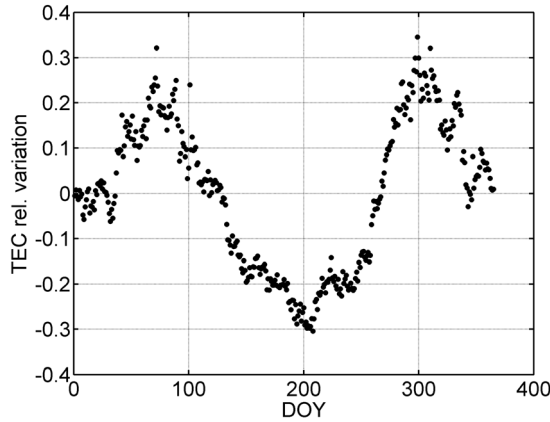


Figure 1. Annual relative variation of the total electron content (TEC) extracted from *Azpilicueta et al.* [2011].

acteristics of the electron density vertical profiles measured by ionosondes. Nevertheless, any new observations that could not be explained by Chapman's theory were considered to be an "anomaly." From this historical perspective, many effects that have been fully explained and modeled with great success are still called "anomalies." The clearest example of this might be the so-called equatorial anomaly, also known as the Appleton anomaly [Appleton, 1946]. However, there are some phenomena that were called anomalies in the early days of ionospheric exploration and have remained as such until the present. Two of the most widely known [see *Fuller-Rowell*, 1998; *Rishbeth*, 1998, 2000; *Li and Yu*, 2003; *Mendillo et al.*, 2005] of these are (1) the semiannual anomaly, which produces larger f_oF_2 values for equinoxes than for solstices; and (2) the annual anomaly (also called the annual asymmetry), which is described by a larger f_oF_2 value during the December than during the June solstice (larger than the 7% that would be expected considering the change in the Sun-Earth distance). Another manifestation of the annual anomaly is the so-called winter anomaly [Appleton, 1938]: f_oF_2 values measured during June over the Northern Hemisphere that are actually lower than (or comparable to) the December values, which is in opposition to the accepted dependence on the Sun's zenith angle.

[6] In an earlier study [Azpilicueta et al., 2011] we presented a technique that was highly successful in reconstructing the annual relative variation that the combined effect of both anomalies has on the daily mean global total electron content (TEC), using TOPEX data measured within the region limited by $\pm 60^\circ$ of geographic latitude. This parameter is defined as the linear integral of the electron density over the vertical, i.e., $\text{TEC}(\lambda, \varphi, t) = \int N_e(\lambda, \varphi, h, t) dh$, and follows a variability pattern similar to that of f_oF_2 . The data used in that work are the outstanding 13 year TEC data series provided by the TOPEX/POSEIDON mission [Fu et al., 1994].

[7] Figure 1 reproduces the main result of that work. Solid diamonds correspond to the annual relative variation of the TEC, $\gamma_{\text{TEC}} \equiv (\text{TEC} - \text{TEC}_0)/\text{TEC}_0$, as a function of the day of the year (DOY), where TEC_0 represents the expected value according to the 11 year solar cycle. Figure 1 clearly

shows the main features of both anomalies: (1) two significant maxima that occur close to the equinoxes and (2) two minima close to the solstices, with the December maximum being larger than the June one.

3. Charged-Particle Magnetic Drifts

[8] Following R. Fitzpatrick et al. (2008, section 2.5), the equation

$$\vec{U}_{1\perp} = \frac{\mu}{m\Omega} \vec{b} \times \nabla B + \frac{U_{0\parallel}}{\Omega} \vec{b} \times \frac{d\vec{b}}{dt} + \frac{\vec{b}}{\Omega} \times \frac{dV_E}{dt} \quad (1)$$

gives the general expression for the magnetic drifts, $\vec{U}_{1\perp}$, that a charged particle experiences at point \vec{r} and time t , within a region with a magnetic field $\vec{B}(\vec{r}, t) = B(\vec{r}, t) \cdot \vec{b}(\vec{r}, t)$, where \vec{b} is a unit vector; $U_{0\parallel}$ is the velocity parallel to \vec{B} that results from the interhemispheric bouncing movement of the particle; and V_E is the velocity that results from the interaction of the particle with electric fields; $\Omega = eB/m$ is the gyrofrequency; m and e are the mass and electric charge of the particle; and $\mu = mu_{\perp}^2/2B$ is the magnetic moment of the particle associated with the gyromotion. It is common to call the terms on the right-hand side of equation (1) grad- B drift, inertial drift, and polarization drift, respectively.

[9] Considering that

$$\frac{d\vec{b}}{dt} = \frac{\partial \vec{b}}{\partial t} + (\vec{V}_E \cdot \nabla) \vec{b} + U_{0\parallel} (\vec{b} \cdot \nabla) \vec{b}, \quad (2)$$

then the inertial drift takes the following form:

$$\vec{U}_{\text{int}} = \frac{U_{0\parallel}}{\Omega} \vec{b} \times \left(\frac{\partial \vec{b}}{\partial t} + (\vec{V}_E \cdot \nabla) \vec{b} \right) + \frac{U_{0\parallel}^2}{\Omega} \vec{b} \times (\vec{b} \cdot \nabla) \vec{b}. \quad (3)$$

When this theory is applied to explain the movement of a charged particle within the magnetosphere, it is common to assume a stationary magnetic field [Rossi and Olbert, 1970; R. Fitzpatrick et al., 2008], $\partial \vec{b} / \partial t \approx 0$, and a weak electric field, $\vec{V}_E \approx 0$; then the inertial drift turns into the so-called curvature drift:

$$\vec{U}_{\text{curv}} = \frac{U_{0\parallel}^2}{\Omega} \vec{b} \times (\vec{b} \cdot \nabla) \vec{b}. \quad (4)$$

On the basis of the latter result, equation (1) is reduced to

$$\vec{U}_{1\perp} \approx \frac{\mu}{m\Omega} \vec{b} \times \nabla B + \frac{U_{0\parallel}^2}{\Omega} \vec{b} \times (\vec{b} \cdot \nabla) \vec{b}, \quad (5)$$

which is the generally accepted expression used to describe the precession drift that a charged particle experiences in Earth's magnetic field, and it is very successful in explaining the existence of the ring current in the region close to the equator. $U_{0\parallel}$ is proportional to the total kinetic energy of the particle and depends on the magnetic latitude, reaching a maximum close to the magnetic equator and vanishing close to the mirror points.

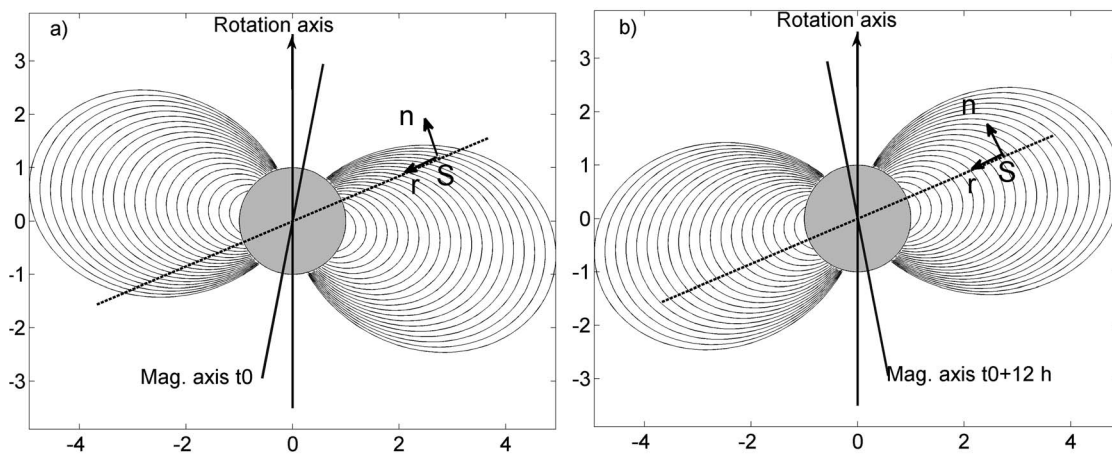


Figure 2. Schematic representation of Earth's rotation and magnetic axes. (a) Axis configuration for a given moment t_0 . (b) Configuration for the moment $t_0 + 12$ h. S is a point in the Sun-Earth direction; r and n are unit vectors defining a nonrotating coordinate system. Concentric curved lines represent the distribution of the geomagnetic field lines for every moment.

[10] One fundamental aspect of equation (5) is that both terms produce precessional drifts, meaning that it does not predict that the particle could move downward; that is, no vertical (radial) drift is possible.

4. Inertial Drift

[11] It is well known that Earth's rotation axis does not coincide with the axis of Earth's magnetic field; they are separated by an angle of $\sim 11^\circ$. From this, the magnetic axis completes one revolution around the rotation axis after 1 day. Figure 2 shows the geometric configuration of the axes for two moments of the day separated by 12 h of universal time (UT). The concentric curved lines represent the distribution of the geomagnetic field lines at every moment.

[12] For the purpose of clarity, let us define a coordinate system that does not rotate with Earth and has the r axis in the Sun-Earth direction pointing toward the center of Earth and the n axis perpendicular to the r axis and pointing to the north pole of Earth's rotation axis. The third axis is defined perpendicular to r and n , pointing to the east and denoted e . Then, at a point fixed in this system the magnetic vector presents a time variation due to Earth's rotation, independent of any additional temporal variation induced by other sources.

[13] Figure 3 shows the direction of \vec{b} (the direction of Earth's magnetic field) every 15 min, in the r and n plane at a point located in the Sun-Earth direction and at a distance of $3 R_E$ (Earth radii) from Earth's center, for DOY 80, 172, 264, and 355, corresponding to equinoxes and solstices alternately. Comparison of the variability between days indicates a clear difference between equinoxes and solstices, and even a difference between solstices. To quantify this, the angular amplitude is $\sim 41^\circ$ for DOY 080 and 264, $\sim 26^\circ$ for DOY 172, and $\sim 31^\circ$ for DOY 355. It is worth pointing out that the magnetic vector also varies in the e direction, but it shows a similar pattern for every DOY.

[14] When the $\partial\vec{b}/\partial t$ term is not neglected in equation (3), equation (1) leads to

$$\vec{U}_{1\perp} \approx \frac{\mu}{m\Omega} \vec{b} \times \nabla B + \frac{U_{0\parallel}^2}{\Omega} \vec{b} \times (\vec{b} \cdot \nabla) \vec{b} + \frac{U_{0\parallel}}{\Omega} \vec{b} \times \frac{\partial \vec{b}}{\partial t}. \quad (6)$$

Equation (6) presents a remarkable difference from equation (5), since the last term has a radial component. This predicts the radial motion of particles, and thus it allows charged particles to cross Earth's magnetic field lines, thus spiraling inward through Earth's magnetosphere, where they may eventually precipitate within Earth's upper atmosphere and ionosphere. The symbol \approx stands for the weak electric field approximation.

[15] The result is that in addition to the bouncing movement of the guiding center between mirrors points and the precession drifts described by equation (5), the charged particle now has an additional drift given by the last term in equation (6):

$$\vec{U}_{\text{int}} = \frac{U_{0\parallel}}{e} \frac{m}{B} \vec{b} \times \frac{\partial \vec{b}}{\partial t}. \quad (7)$$

In the particular case of a charged particle performing the precessional drifts given by equation (5) and considering a reference system that is not rotating with Earth, equation (7) gives the inertial drift followed by the particle. As mentioned in section 1, the term $\partial\vec{b}/\partial t$ is a consequence of the $\sim 11^\circ$ tilt angle between Earth's magnetic and Earth's rotation axes.

[16] Equation (7) can be split into two terms: The first one, $U_{0\parallel}m/e$, depends on the total kinetic energy of the particle and acts as a scale factor with a maximum value close to the magnetic equator. The dependence on e indicates that the ions and electrons have inertial drifts with opposite directions. The second term,

$$\vec{u} \equiv \frac{1}{B} \vec{b} \times \frac{\partial \vec{b}}{\partial t},$$

is a vector magnitude that depends on \vec{r} and t .

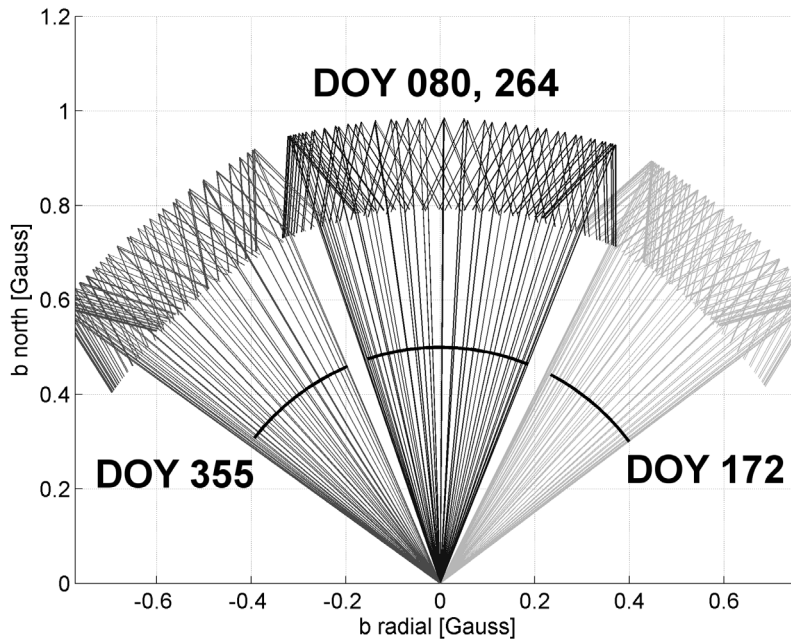


Figure 3. Earth’s magnetic vector temporal variation. Variation along 1 day of the direction of Earth’s magnetic vector on the r - n plane, at a point located in the Sun-Earth direction and at a distance of $3 R_E$ from Earth’s center. Different degrees of gray shading correspond to days of the year (DOY) 080, 172, 264, and 355.

[17] To simplify the study of the effect of equation (7), time-average values every half hour were computed. This is a very common practice in describing the movement of a charged particle in a magnetic field, and although it is an approximation, it is very useful for understanding the way in which the particle trajectory is modified by the new term.

[18] To pursue the analysis, equation (7) was evaluated at two points lying in the Sun-Earth direction at two different distances using the International Geomagnetic Reference Field 10 (IGRF10) [Macmillan and Maus,

2005]. Figure 4a shows the radial component of \vec{u} computed as a function of UT for a distance of $3 R_E$. Each curve (identified by different symbols) corresponds to a different DOY: 80, 172, 264, and 355. This distance approximately represents the location of the inner radiation belt, and Figure 4b corresponds to a distance of $0.2 R_E$, thus representing approximately the upper height limit of the ionosphere.

[19] There are several interesting features in Figure 4.

[20] 1. A positive value means a downward velocity component for ions (and the opposite for electrons) and

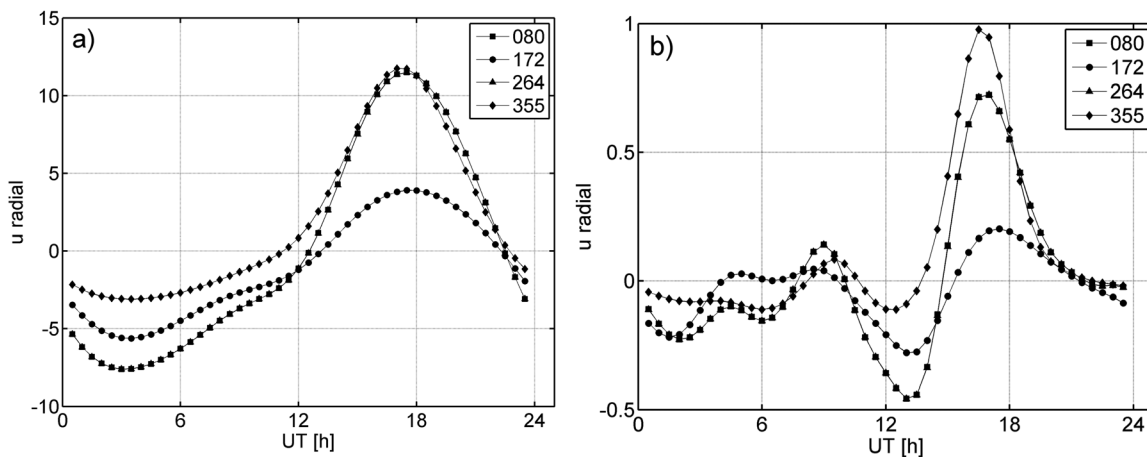


Figure 4. Differential effect of the Earth rotation dynamo force (ERDF) along the year. Radial component of \vec{u} versus universal time for DOY 080, 172, 264, and 355 at a distance of (a) $3 R_E$ and (b) $0.2 R_E$. The series for DOY 080 and 264 is superimposed.

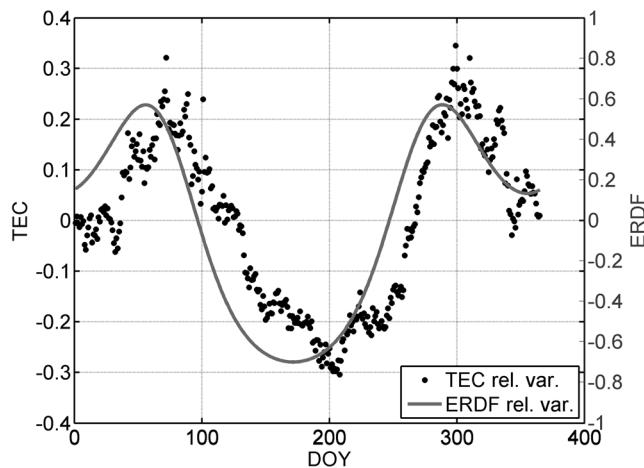


Figure 5. ERDF kinetic energy transfer along the year. The solid line represents the annual relative variation owing to the ERDF energy variation as a function of DOY. Solid diamonds represent the annual relative variation of the TEC.

indicates that the model predicts the radial motion of ions. This inward motion of ions may lead to their precipitation within the upper atmosphere and ionosphere.

[21] 2. Although Figure 4 shows the behavior at two selected distances, the effect is present over all distances in between.

[22] 3. The peak in the curves close to 1600 UT tends to be more significant, within the day, as the distance to Earth decreases.

[23] 4. The curve that corresponds to DOY 172 (June solstice) shows the minimum min–max range.

[24] To understand point 3, it is worth noting that for the period between 1400 and 1800 UT the Sun–Earth direction crosses the region that corresponds to the South Atlantic anomaly [Abdu *et al.*, 2005] of Earth’s magnetic field. The explanation for point 4 is that for approximately DOY 172 the Sun–Earth direction reaches the largest angular distance from the center of the South Atlantic anomaly, and thus its influence is significantly reduced.

[25] The previous considerations show that the trajectory of charged particles (ions) of the radiation belt is not exactly a ring but a spiral carrying them inward until they penetrate Earth’s upper atmosphere. The driving force of this effect is a dynamo force due to the tilt angle between Earth’s magnetic and its rotation axes, already defined as the ERDF.

5. Kinetic Energy Considerations

[26] The daily average kinetic energy, per unit of mass, transferred by the ERDF to a charged particle can be deduced from equation (7) as

$$K_{\bar{U}_{\text{int}}} = \frac{1}{2} \left\langle \left| \frac{U_{0\parallel} m}{e} \right|^2 \|\bar{u}\|_2^2 \right\rangle,$$

where angle brackets represents the daily average. The solid line in Figure 5 shows the relative annual variation

$$\gamma_{K_{\bar{u}}} = \frac{K_{\bar{u}} - \tilde{K}_{\bar{u}}}{\tilde{K}_{\bar{u}}} \text{ of } K_{\bar{u}},$$

where $\tilde{K}_{\bar{u}}$ is the annual mean, as a function of the DOY, at a point located in the Sun–Earth direction at a distance of $0.2 R_E$. For computation of this series we made the approximation that the behavior of $|U_{0\parallel}|$ is the same for every DOY. The pattern shown by the curve is remarkable in the sense that it shows two quite pronounced maxima, approximately coincident with the equinoxes, and two asymmetric minima in the solstices.

6. Earth Rotation Dynamo Force Energy Transfer

[27] Chaman Lal studied the semiannual ionospheric anomaly from an energetic point of view and concluded that a secondary source of energy was essential, acting in addition to the solar radiative input [Lal, 1997]. In that work the author proposed that the extra energy was provided by charged particles from the ring current that descend until reaching the upper atmosphere, although he could not specify the actual physical mechanism involved. From this point of view, the annual relative variation of the TEC can be considered as the annual relative variation of the energy required (from the secondary source) to enhance the mean electron density of the ionosphere with respect to the mean annual value. Solid diamonds superimposed in Figure 5 represent this series.

[28] The similarity between the annual relative variations of the TEC, γ_{TEC} , and the ERDF kinetic energy annual variation, $\gamma_{K_{\bar{u}}}$, is remarkable and provides evidence in favor of Chaman Lal’s hypothesis. It is important to remember that both series were obtained from completely independent principles: The γ_{TEC} is experimental and was obtained from TOPEX TEC direct determinations for a period of 13 years, while the γ_K was obtained based on the ERDF theoretical model using equation (7), Earth’s magnetic field given by the IGRF10, and the change in the Sun–Earth direction throughout the year.

7. Solar Wind Considerations

[29] A closer examination of Figure 5 indicates that both series do not match exactly, since (1) there seems to be a time shift between them, and (2) the shapes are quite similar but not identical (a constant time shift does not solve the problem).

[30] The hypothesis of nonradial flow of the solar wind has been studied in the past year [Richardson *et al.*, 2009]. One hypothesis is that in the region close to the Sun’s magnetic equator, the solar wind vector direction mainly flows parallel to it (i.e., parallel to the Sun’s magnetic field lines), while for regions away from it, the solar wind vector tends to flow in the radial direction. Assuming this hypothesis, the direction of preference, i.e., the Sun–Earth direction, can be replaced by the one parallel to the solar wind. After reproducing the work described in the section 6, we reach the outstanding result plotted in Figure 6: The shift and shape difference have now disappeared, and both series match in time and shape.

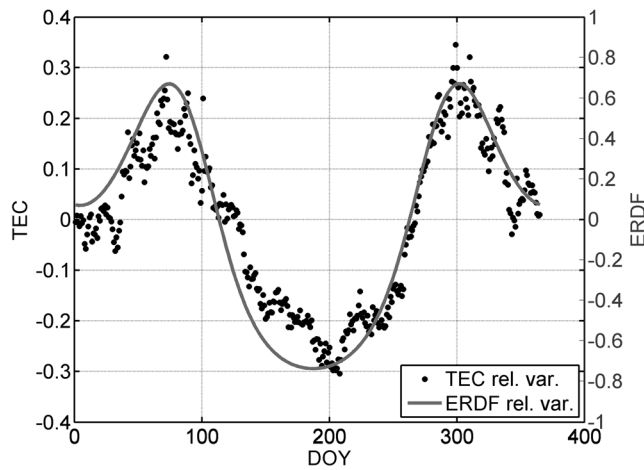


Figure 6. ERDF kinetic energy transfer along the year: solar wind parallel to the Sun's equator. The solid line represents the annual relative variation owing to the ERDF energy variation as a function of DOY. Solid diamonds represent the annual relative variation of the TEC.

[31] In considering this issue it is important to note that the maximum angular separation between the two directions mentioned in the previous paragraph is only $\sim 7^\circ$.

8. Conclusions

[32] During the past decades the widely used assumption that at a fixed point within the magnetosphere $\partial b/\partial t \approx 0$ has led to simplifying the inertial magnetic drift to the curvature precession drift alone, thus limiting the ability of the theory to fully describe the movement of the charged particles within Earth's magnetosphere. When the $\sim 11^\circ$ tilt angle between Earth's rotational and its magnetic axis is considered, these effects cannot be neglected, and thus an additional force, the ERDF, acts on the charged particles.

[33] On the basis of the complete inertial drift formula, we have now developed a model that provides a mechanism by which charged particles from the ring current may be transferred to the upper atmosphere and ionosphere. The transfer process is not uniform throughout the year; it is a function of the DOY.

[34] Next we have shown that the semiannual and annual anomalies observed in the annual relative variation of the ionospheric TEC could be explained by a unique process that involves energy transfer from the ring current to the atmosphere. The additional energy for the day, i.e., the energy not related to solar electromagnetic radiation, is regulated by the ERDF and it thus depends on the DOY. This energy is absorbed by the atmosphere and, by a still unidentified process (ionization, dissociation, and thermal excitation are possibilities), can produce the observed electron density variations. The most important evidence that supports this statement is the remarkable similarity between the annual variations of γ TEC and those of ERDF shown in Figure 6. A rather fascinating result is that when, in the equations, the Sun-Earth direction is replaced by the solar wind radial direction, the matching of the series is almost perfect.

[35] Finally, in this work we have only considered the consequences of applying the ERDF theory to particles in the ring current, but the effect is also present in the outer region of the magnetosphere. Presently, a similar study is being carried out for the region between the plasma pause and the inner radiation belt. The results are encouraging in the sense that the ERDF theory can explain the observed semiannual and annual anomalies and provide a continuous mechanism to replenish the ring current with charged particles from the solar wind. These results will also help us to better understand the influence of the solar wind direction on the phenomena studied in the present work.

[36] **Acknowledgments.** The authors thank Sandro Maria Radicella for his assistance in understanding the TEC anomalies and Ana Maria Platzeck for the discussions about the problem of charged-particle magnetic drifts. The authors are very grateful to the two anonymous reviewers, whose comments significantly enhanced the quality of this paper. F. Azpilicueta thanks the Universidad Nacional de La Plata-Abdus Salam International Center for Theoretical Physics Federation Agreement for funding the first part of the research involved in this work.

[37] R. Lysak thanks Ildiko Horvath and another reviewer for their assistance in evaluating this paper.

References

- Abdu, M. A., I. S. Batista, A. J. Carrasco, and C. G. M. Brum (2005), South Atlantic magnetic anomaly ionization: A review and a new focus on electrodynamics effects in the equatorial ionosphere, *J. Atmos. Sol. Terr. Phys.*, *67*, 1643–1657.
- Appleton, E. V. (1938), Radio transmission and solar activity, *Nature*, *3594*, 142, 499–501.
- Appleton, E. V. (1946), Letter: Two anomalies in the ionosphere, *Nature*, *3995*, 691.
- Azpilicueta, F., C. Brunini, and S. M. Radicella (2011), Semi-annual anomaly and annual asymmetry on TOPEX TEC during a full solar cycle, in *Proceedings of 2009 IAG Scientific Meeting*, in press.
- Berkner, L. V., H. W. Wells, and S. L. Seaton (1936), Characteristics of the upper region of the ionosphere, *Terr. Magn. Atmos. Electr.*, *41*(2), 173–184.
- Chapman, S. (1931), The absorption and dissociative or ionizing effect of monochromatic radiation in and atmosphere on a rotating Earth: part II. Grazing incidence, *Proc. Phys. Soc.*, *43*, 483–501.
- Fu, L.-L., E. Christensen, C. Yamarone, M. Lefebvre, Y. Menard, M. Dorrer, and P. Escudier (1994), TOPEX/POSEIDON mission overview, *J. Geophys. Res.*, *99*(C12), 24,369–24,381.
- Fuller-Rowell, T. J. (1998), The “thermospheric spoon”: A mechanism for the semiannual density variation, *J. Geophys. Res.*, *103*(A3), 3951–3956.
- Lal, C. (1997), Contribution to F_2 layer ionization due to the solar wind, *J. Atmos. Sol. Terr. Phys.*, *59*(17), 2203–2211.
- Li, X., and T. Yu (2003), Annual and semi-annual variations of the observed f_oF_2 in a high solar activity year, *Terr. Atmos. Oceanic Sci.*, *14*(1), 41–62.
- Macmillan, S., and S. Maus (2005), International Geomagnetic Reference Field—The tenth generation, *Earth Planet Sci.*, *57*, 1135–1140.
- Mendillo, M., C. Huang, X. Pi, H. Rishbeth, and R. Meier (2005), The global ionospheric asymmetry in total electron content, *J. Atmos. Sol. Terr. Phys.*, *67*, 1377–1387.
- Richardson, J. D., E. C. Stone, J. C. Kasper, J. W. Belcher, and R. B. Decker (2009), Plasma flows in the heliosheath, *Geophys. Res. Lett.*, *36*, L10102, doi:10.1029/2009GL038421.
- Rishbeth, H. (1998), How the thermospheric circulation affects the ionospheric F_2 layer, *J. Atmos. Sol. Terr. Phys.*, *59*, 1385–1402.
- Rishbeth, H. (2000), The equatorial F layer: Progress and puzzles, *Ann. Geophys.*, *18*, 730–739.
- Rossi, B., and S. Olbert (1970), *Introduction to the Physics of Space*, McGraw-Hill, New York.

F. Azpilicueta (corresponding author) and C. Brunini, Facultad de Ciencias Astronómicas y Geofísicas, Universidad Nacional de La Plata, Consejo Nacional de Investigaciones Científicas y Técnicas (CONICET), Paseo del bosque s/n, 1900 La Plata, Argentina. (azpi@fcaglp.unlp.edu.ar)